

# Scattering Spectroscopy of Plasmonic Janus Particles

Felix H. Patzschke and Frank Cichos\*

*Molecular Nanophotonics Group, Peter Debye Institute for Soft Matter Physics, Leipzig University, 04103 Leipzig, Germany*

E-mail: cichos@physik.uni-leipzig.de

## Abstract

Plasmonic Janus particles consist of dielectric core particles with a thin metallic cap on one side and are widely used in active matter research.<sup>1</sup> The plasmonic cap enhances optical scattering and absorption, allowing for self-propulsion through temperature gradients as well as efficient trapping and tracking.<sup>2,3</sup> The asymmetry of such a particle gives rise to surface plasmon modes whose excitation is sensitive to the angle at which the particle is illuminated. Even though the angle of illumination strongly influences the particle's scattering response, the optical properties of such metallic caps have hardly been investigated.

We probe the light scattering of individual micrometre-sized, spherical, Au-coated Janus particles by means of Selective Illumination Multiplexed Fourier Plane Spectroscopy. This novel method allows us to explore micro-particles' scattering characteristics resolved for wavelength, angle of illumination and scattering angle.

In addition, we supplement our experimental results with finite-element simulations and correlate spectral markers to orientation-dependent surface plasmon modes. This additional information on the correlation of angular and spectral information could pave the way for new methods of orientation detection. They also shed new light on the interaction of such spherically capped particles with light inducing forces and torques.<sup>4,5</sup>

## Keywords

Janus Particle, Fourier Optics, Spectroscopy

# Introduction

Janus particles (JPs) with a plasmonically active cap are a widely-used tool in active matter research<sup>1</sup>: Through the absorption of visible light, the cap can be heated efficiently. In conjunction with the anisotropy of the particle, this facilitates directed self-propulsion<sup>2,3</sup>. [to do: citations] Meanwhile, the enhanced optical scattering of the cap leads to good visibility in microscopy, particularly in the dark field, which, in turn, allows for accurate tracking of the motile particles. [to do: citations] In conjunction, these two properties enable real-time feedback applications. [to do: citations]

As widely applicable as these particles' light-matter interactions (LMIs) may be, they are certainly not trivial: The length scales of the surface curvature are in the same order of magnitude as the wavelengths of light in the interaction, such that approximations along the lines of ray optics or dipole scattering must be assumed invalid. In addition, the asymmetry of the particles leads to orientation-dependency of the LMI. These orientation-dependencies may manifest in counter-intuitive ways: For instance, numerical studies have suggested that plasmonic JPs can stably rotate, powered by a linearly polarized light field.<sup>4,5</sup>

For a decade and a half, spectroscopy has been established as the choice tool for probing the anisotropic LMIs of small plasmonic scatterers with [more complicated than spherical] geometry<sup>6,7</sup>. A wide range of particles, such as nanorods and -triangles<sup>8</sup>, nanoparticle aggregates<sup>9</sup> and substrate-bound nano-cups<sup>7,10</sup>, has been studied. For the most part, research has focused on scatterers that were significantly smaller than the wavelength of probing light<sup>7-9</sup>.

[to do: We extend similar methods to larger particles]

[to do: The value of single-particle measurability]<sup>11</sup>

As a first step towards an understanding of such effects, we study the scattered light from these JPs. We measure scattering spectra of individual JPs while varying the direction of illumination as well as resolving for the scattering

angle. While orientation-dependent scattering studies of plasmonic nanostructures *have* been performed, that has only been the case for Au nanostructures significantly smaller than the observation wavelengths<sup>8,10,12</sup>. [to do: Halas et al.] As such, no regard was given to the angular distribution of the scattered light. In our studies of micrometre-sized JPs in visible and NIR light though, we find that the difference in shape of these distributions can lead to drastic, qualitative differences in measured scattering spectra.

We present an experimental method [to do: based on BFP imaging, Fourier optics + optical spectroscopy<sup>13,14</sup>], which we use to study the LMI of plasmonic JPs consisting of a spherical polystyrene (PS) particle, 1  $\mu\text{m}$  in diameter, with a 50 nm thick gold layer as the cap. We resolve the intensity of scattered light for wavelength and scattering angle. Though the theory of Mie<sup>15</sup> only makes predictions for maximally symmetric particles, it serves well as reference in the characterization of the LMI of plasmonic JPs.

We complement the measurement results with numerical simulations and find a good match between both methods' results. Through the analysis of the simulation results, we correlate peaks in the scattering spectra to orientation-dependent surface plasmon modes.

## Experimental Method

The imaging setup is sketched in Figure 1A. A standard dark-field microscope, constructed around an OLYMPUS IX71 microscope base, was coupled into a selector optic that could be set to propagate either the real-space image, i.e. the sample plane, or the image in the back aperture of the objective (B3) onto a known optical plane. From this plane, a thin vertical strip would be selected via an adjustable slit (B5) to be imaged onto an sCMOS camera sensor. A set distance before the sensor, a transmission grating was placed to spectrally disperse the image from behind the slit. An optical long-pass filter could be inserted to impose a known lower bound on the wavelengths of light being

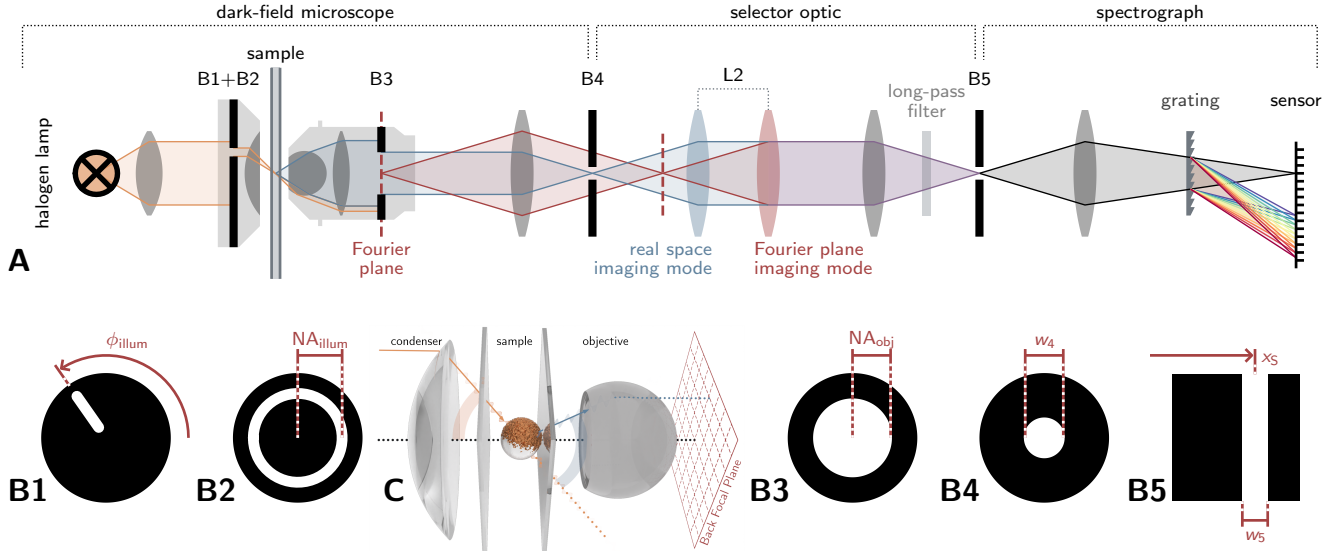


**Figure 1:** **A:** Imaging light path. **B1-B5:** Schematics of the apertures. B1-B3 lay in Fourier planes, B4 lies in an image plane. Depending on the placement of the lens L2, either the image plane or the Fourier plane may be imaged onto B5, and subsequently the camera sensor. **C:** In the immediate vicinity of the particle under observation, the ambient refractive index is virtually homogenous, due to the usage of immersion oil inside the sample.

analyzed, thus giving a known upper bound for the validity of measurements, beyond which the measured intensity distributions would overlap with the second interference order.

The real-space-imaging mode was used to select particles for measurement as well as for spectral measurements in which the scattering angle was not resolved. The BFP-imaging mode was used to record spectrally resolved Fourier-space scattering maps of the JP under observation. To that end, the slit (B5) was slowly translated across the BFP image while recording an image sequence, such that the camera would record one spectrally dispersed vertical line of the BFP image at a time. This step being the spatio-temporal multiplexing of the line-wise spectral signals, the corresponding de-multiplexing is done later, by appropriately re-arranging the intensity data from the image stack. [to do: This procedure is described in detail in the supplementary material and in<sup>16</sup>.] The accumulation time for one such dataset was approximately 15 minutes.

The JPs consisted of spherical PS beads, coated with a layer of gold, 50 nm thick on average, on one side, with a 5 nm thick layer of chro-

mium as a binding agent in between. A 30  $\mu\text{l}$  droplet was placed on a cover slip and the JPs in solution were left to sediment for 10 minutes. Afterwards, the solvent was blown off using nitrogen gas, leaving the remaining JPs stuck on the coverslide. A second cover slip was placed on top, with a droplet of 1.5  $\mu\text{l}$  of immersion oil in between, such as to keep the ambient refractive index constant in the vicinity of the particles. (see Figure 1C)

## Validation

In order to validate the experimental scheme, we measured the scattering spectra of 65 nm AuNPs. In figure 2A, the measured scattering spectra are shown together with the prediction from Mie theory<sup>15</sup>, computed using the values by Johnson & Christy<sup>18</sup> for the complex refractive index of gold.

We decided on the use of these particles that are much smaller than the JPs we were planning on studying, because the expected resonance peak in the scattering spectrum would be as narrow as possible, giving a good indication as to the spectral resolution of the measurement.

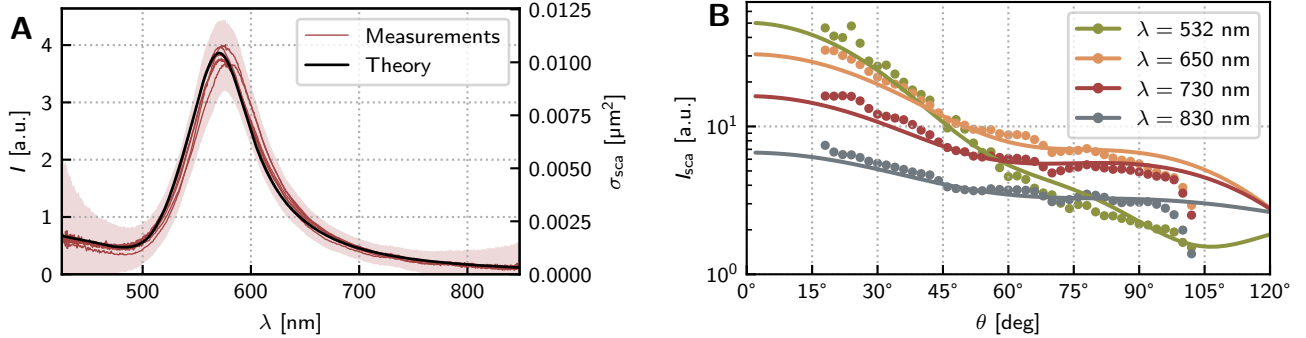


**Figure 2:** Validation measurements. **A:** Scattering spectrum of 65 nm Au NPs. The shaded area corresponds to the maximum noise in the measurements. **B:** Scattering intensity of a spherical Au NP ( $d = 250$  nm) versus the scattering angle for various wavelengths. The lines show the predictions of GLMT<sup>17</sup>, scaled by a constant factor to match the points showing the measurement results.

We find a good match between the measured and theoretical spectra. As the particles were significantly smaller than any probing wavelength, the scattered field is well-approximated by a dipole field. Hence, the shape of the angular distribution of scattered light did not change appreciably over the spectral range of interest, causing the measured and full scattering cross-sections to only differ by a constant factor. Nonetheless, we observe that the peaks of the measured scattering spectra are shifted towards the red end of the spectrum by  $3.6 \pm 2.2$  nm w.r.t. the theoretical result. This is caused by the slightly flatter intensity distribution at longer incident wavelengths.

The flattening of the angular distribution as the wavelength increases is much easier to spot with larger test particles: To validate the BFP spectroscopy, we chose Au particles with a diameter of 250 nm.

The choice of these larger particles was also due to their much greater brightness in the dark field: In the BFP measurement, the scattered light is distributed over a larger area on the sensor, lowering the SNR. The greater scattering cross-section of larger particles remedies that issue. Nonetheless, the scattering cross-section of one such AuNP could be expected to be smaller than that of a JP as used later-on, implying that, if the measurement was valid for the AuNPs, it would also be for the JPs.

The results are shown and compared to the predictions of GLMT<sup>17,19</sup> [Generalized Lorentz-

Mie Theory] in figure 2B. Again, we find good agreement between experiment and theory.

## Dark-Field Spectra

Recorded scattering spectra of the JPs are shown in figure 3, along with numerical predictions. The results from both methods agree reasonably well, with the measured curves falling within a standard deviation of the average of the numerically obtained spectra for the most part.

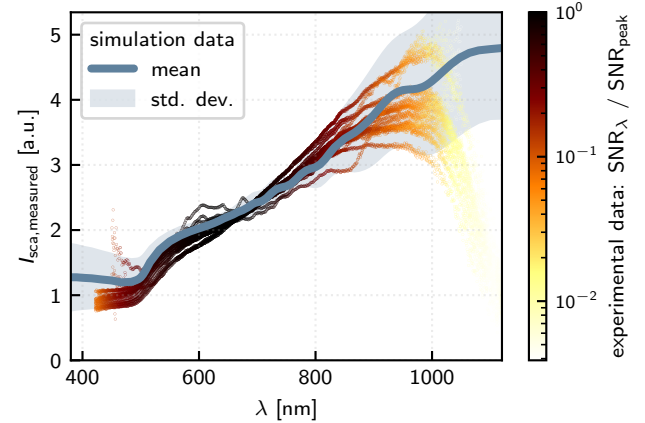


**Figure 3:** Measured scattering spectra (orange) atop value range as determined by simulation + emulation (blue).

All spectra have a recognisable shoulder at 550 nm. A similar feature exists in the scattering spectra of similar-sized Au spheres. We attribute this to the LSPR of gold, though

the otherwise increasing characteristic of the spectra diminishes the distinct peak that it would produce in the scattering spectra of small AuNPs into a mere bump. For longer incident wavelengths, we generally observe the scattering intensity to monotonously increase.

Between 900 and 1000 nm, the degraded efficiency of the measurement setup causes the relative influence of bleed light and sensor noise to increase, rendering the measurements increasingly unreliable. Hence, the measured spectra diverge from one another. The numerical results suggest that the trend of approximately linear increase should continue.

In the numerical calculation of these spectra, we take into account the limited angular collection range of the objective. (For details, see the Supplementary Information)

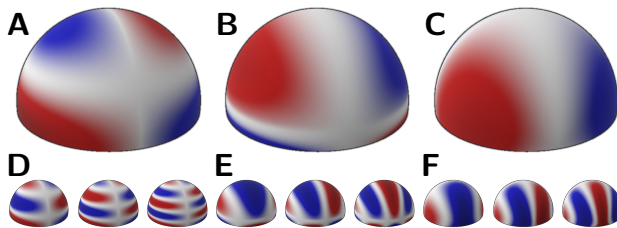


**Figure 4:** Fundamental surface plasmon modes of the JP's cap. **A:** Axial  $\vec{k}$ , **B:** transverse  $\vec{k}$  with axial  $\vec{E}$ , **C:** transverse  $\vec{k}$  with transverse  $\vec{E}$ . **D-F:** corresponding second, third and fourth overtone.

Neither in the measured, nor in the numerically obtained spectra were we able to discern any obvious features that we could relate to an orientational parameter of the system: Under unmodified dark-field illumination, the incident light field is comprised of a superposition of plane waves propagating in different directions simultaneously, exciting a combination of surface plasmon modes in the Au cap of the JP. The hemispherical surface of the cap supports three basic surface plasmon modes, split by the direction of the charge density oscillation (see figure 4), as well as overtones due to the relatively large size of the structure w.r.t. the probing wavelengths.

[ For  $k \ll R_{JP}^{-1}$  (like in previous research), there are only two dipole modes, transverse-electric (A&C) and polar-electric (B). The transverse-electric mode is twice degenerate, as

the electric field may oscillate in either the  $x$  or the  $y$  direction. As  $k \cdot R_{JP}$  grows large enough for the outside electric field to change not only w.r.t. time but also a spatial coordinate, the next pure surface plasmon modes are quadrupole modes. (Figure 4A-C) The previous transverse-electric mode is split into a polar- $k$  (A) and a transverse- $k$  (C) mode. The polar- $k$  mode is further degenerate, as, here, the electric field may still oscillate in either the  $x$  or the  $y$  direction. ]

## Dark-Field Spectra under Selective Illumination

We inserted the aperture B1 to restrict the direction of illumination to a very small angular range ( $\Omega = 0.096 \text{ sr}$ ) [to do: check!]. This allows us to do the first step of disentangling the surface plasmon excitations.

In figure 5 (left), we show dark-field images of an individual JP, illuminated from different directions. The apparent brightness of the JP in the dark field depends heavily upon the direction of illumination. For shorter wavelengths, this includes multiple pronounced local minima and maxima. For longer wavelengths, these local extrema are diminished.

[to do: Particle appears much brighter when illuminated from the Au side. It stands to reason that its out-of-plane orientation made it such that when the aperture was rotated such that the PS side would be illuminated, the light *actually* hit side-on. (I.e. cap pointing ca. 30° up towards the condenser)]

## Scattering Spectra

Using the real-world optical setup, it is not possible to capture all of the scattered light. However, we can readily extract predicted values of the scattering cross-section of the JP from the simulations: With the illumination angle as a parameter, we obtain a family of scattering spectra,

$$\zeta \mapsto [\lambda \mapsto \sigma_{\text{sca}}] ,$$

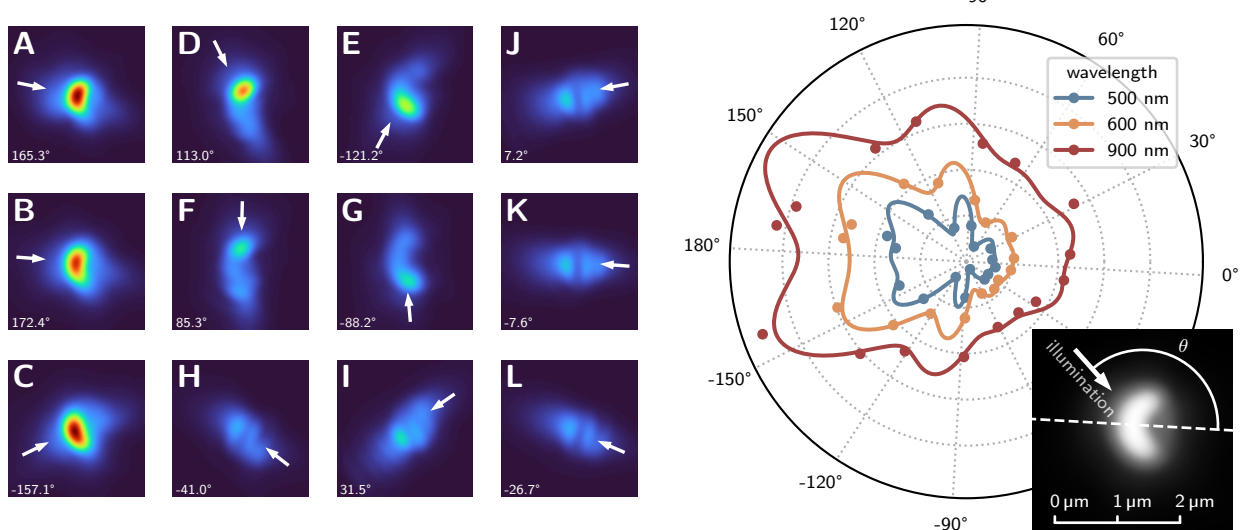


**Figure 5:** Dark-field images of a JP under selective illuminations. The respective in-plane angles are noted in the lower left corner.

each spectrum  $\lambda \mapsto \sigma_{\text{sca}}$  corresponding to a specific illumination angle  $\zeta$ . Figure 6A shows the scattering spectra for the maximally symmetric orientations of  $\zeta = 0$  and  $\zeta = \pi$ , as well as for  $\zeta = \pi/2$ , i.e. the case wherein  $\hat{k}_0 \perp \hat{z}$ . A scattering intensity map, taking into account other sampled illumination angles is shown in [to do: supplementary figure].

The scattering spectra differ significantly from the measured dark-field spectra, though some correspondences between features can be inferred: The previously noted increasing trend is, once again, present, as is the sharp upward bend at 500 nm. However, [to do: distinct wobbles for  $\lambda > 600$  nm, decrease of scattering cross-section up to the minimum at 500 nm]

Within the visible part of the spectral range, the increase of the scattering cross-section coincides with that of the measured intensities. In the NIR range, the measured brightness increases further; this is due to the broadening of the forward scattering peak.

For wavelengths beyond 700 nm, the scattering cross-sections, between illumination from the Au side and from the PS side, are virtually the same. They are, moreover, significantly larger than that for side-on illumination, on average. However, at  $\lambda = 1210$  nm, they have a local minimum where the scattering cross-

section is less than that for side-on illumination. This points at a polar plasmon mode that is being excited out-of-phase. [to do: Explain better what I mean.] [Curiously, the peaks in the absorption spectra don't line up with either the valleys or the peaks in the scattering spectra. They don't for AuNPs either.]

This is due to only scattered light which is emitted in such a direction that it is collected by the objective contributing to the measured scattering intensity, while the simulated scattering spectra take into account the energy flow density of the scattered field itself.

[The average of ] The thus computed spectra reproduce the measured dark-field spectra well. [most of the individual sample spectra fit reasonably well but there are some outliers. The average fits nicely, but ultimately one of those samples is likely the truth. And they have the same limitations in regards to details lost.] Meanwhile, details such as the local maxima of the full scattering spectra are lost. [to do: with the possible exception of a small wobble at 850 nm, but it's unclear how exactly it arises. Maybe it's the  $k = \pm 4$ -peak?]

[to do: We find that the scattering cross-section heavily depends on the orientation of the JP.] Over the spectral range that we analyzed, though decidedly not in general, the scat-

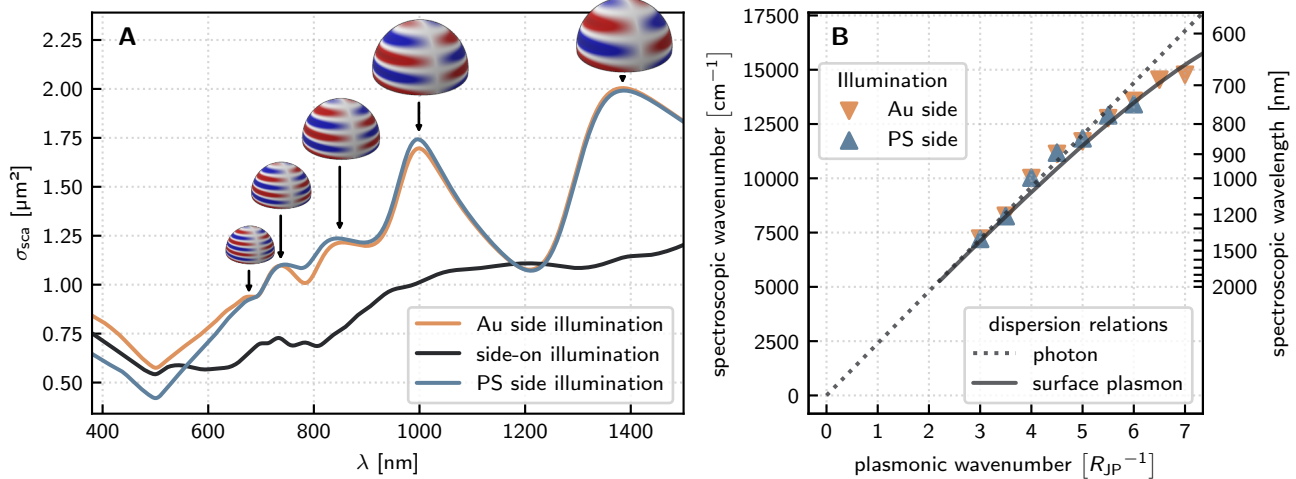


**Figure 6:** **A:** Simulated scattering spectrum of the JP under illumination from the Au side (yellow), from the PS side (blue) and from the equatorial side (black). **B:** Excitation wavelengths of peaks and valleys in the axial illumination scattering spectra vs. spatial frequency of the electric field on the surface of the Au cap.

tering efficiency of the particle was ... greater if it was illuminated from either the Au or the PS side than if it was illuminated side-on. In both cases, the scattering spectra have multiple peaks. Between axial and side-on illumination, though, there is no clear correspondence between these peaks.

E.g., for side-on illumination, there is a scattering peak at  $\lambda \approx 550 \text{ nm}$ , that has no counterpart in the spectra for axial illumination. We ascribe this peak to the nanostructure plasmon resonance of gold: It sits right around that wavelength and it is only under side-on illumination that the incident electric field may be perpendicular to the surface of the Au cap at its points of highest curvature, that being the cap's perimeter.

The bump at  $\lambda \approx 550 \text{ nm}$  is discernable in both real and emulated measurements, while only appearing in the raw scattering cross-sections for side-on illumination. Notably, this peak occurs at the same wavelength as the main LSPR for an arbitrarily small AuNP. We reason that this plasmon is excited in the rim of the cap by electric fields that are perpendicular to the Au surface in its regions of maximal curvature.

Conversely, the peak at  $\lambda \approx 996 \text{ nm}$  is present under just the opposite circumstances, i.e. when  $\hat{k} \parallel \hat{z}$ . For these orientations, the

system is rotationally symmetric in the polarization average and the surface plasmon propagates along the polar direction on the Au cap, inward for  $\zeta = 0$  and outward for  $\zeta = \pi$ . A quantity akin to a wave vector can be assigned to the polar surface plasmon mode, by counting the sign changes of the surface charge density on a geodesic path from the apex of the cap to its rim. For the 996 nm peaks, this means  $\tilde{k} = \pm 3$ . [to do: Similarly, we can assign such a pseudo wave vector to all the other peaks in the scattering spectra for axial illumination. The result is Figure 6B.]

[to do: Proper analysis of the surface plasmon wavevector stuff.]

Neither of these peaks is present [discernable?] in the scattering spectrum of an equivalently sized Au sphere. This implies that [to do: either] the associated surface plasmon modes do not exist on a closed sphere in this form [to do: or the AuS spectrum is more closely related to the orientation-average of the JP spectra than it is to any single one of them].

[to do: peaks and valleys correspond to only peaks on AuNPs → proximity of peaks makes them unresolvable]

The weak scattering of even-numbered resonances is due to the surface charge density having opposite signs in corresponding areas of the in-

side and outside of the gold cap. Whether the same effect could be observed on a core-shell particle of equivalent size is unclear: On one hand, it has been suggested that light interaction properties of JPs can be approximated as a mix between those of solid particles and of core-shells [to do: Citation: black paint]. On the other hand, visual inspections of the time-dependent solutions for the electric field suggest that the surface charge densities on the in- and outside of the cap are coupled via the boundary of the cap rather than through transmission through it. This would imply that the odd-even splitting would not happen on a CS particle, as transmission through the Au layer would be the only possible way of coupling the inside field to the outside one.

[to do: For side-on illumination but arbitrary polarization, there is also something happening on the cap, not just on the rim. Would that be an extra class of modes? (let's call 'em longitudinal to distinguish them from the polar and azimuthal modes) And are those the tiny peaks in the side-on scattering spectrum between 650 and 850 nm?]

Comparing the angular distributions to those of a Mie particle though, there is clear similarity: Non-global maxima become more well-distinguished and fewer in number as wavelength increases. The same happens as the direction of illumination is changed from  $\hat{k} \perp \hat{z}$  to  $\hat{k} \parallel \hat{z}$ : Both parameter changes can, from a Mie-theoretical point of view, be understood as a decreasing size parameter and thus the transition from the ray optics regime ( $\lambda \ll R$ ) to a dipole model ( $\lambda \gg R$ ).

[to do: The out-of-plane orientation of the JP is not easy to infer: None of the spectral features that signify a specific illumination angle are resolvable. ...] The spectral peaks that are characteristic to each orientation are not recognizable in a measurement. [to do: how to make them visible?]

[to do: A summary figure of sim results: scattering spectra, Mie plots and the like]

## Fourier Plane Spectra

In the multiplexed Fourier plane spectroscopy, the angular distributions of the scattering intensity became visible. We performed measurements under three different settings of the selective illumination, each chosen to match as closely as possible the cases of Au-side, PS-side and side-on illumination. Because the exact out-of-plane angle of the particle under observation is unknown and in order to allow for easier comparison of measured and numerical data, we extracted 1-dimensional intensity profiles along the polar coordinate from the Fourier plane images. Measured and simulated scattering profiles are shown in Figure 7.

For all illumination directions, most of the scattered light is only lightly deflected off of the propagation direction of the incident light. However, there were qualitative distinctions between the distributions that hold over the entire spectral range under consideration: The peak brightness was highest for illumination from the Au side, while a wider peak and significant sideways scattering accumulated into a greater absolute brightness under illumination from the PS side.

The behaviours described also hold true for the full images.

Unsurprisingly, the distributions were symmetric about the axis of illumination. This was not the case for the side-on illumination, where light was preferentially scattered in the direction of the Au side.

The simulated far-field patterns show the same results.

[to do: Discussion about the angular distributions - Lift something from the MA.]

## Conclusion & Outlook

[to do: Method] In summary, we have demonstrated *Selective Illumination Multiplexed Fourier Plane Spectroscopy*, a technique by use of which the optical scattering from individual micrometre-sized plasmonic structures can be measured w.r.t. wavelength and scattering angle. This technique was applied to probe the

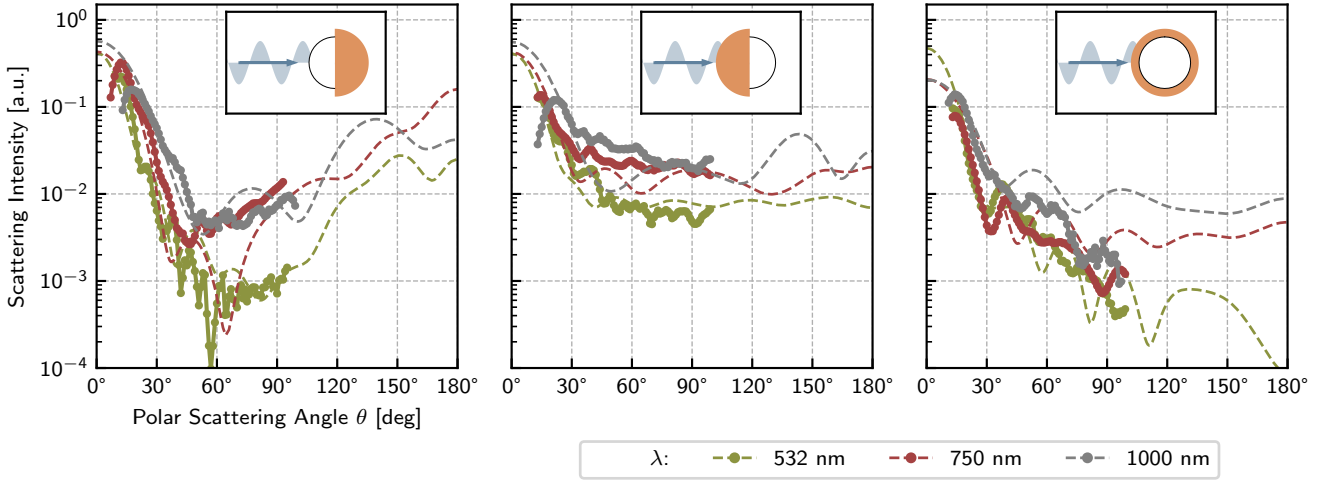


**Figure 7:** Scattering intensity of the JP versus scattering angle for various wavelengths. The points correspond to measured intensities while the lines are simulation results. **A:** PS side illumination. **B:** Au side illumination. **C:** side-on illumination.

orientation-dependent light scattering of Au-coated Janus particles. [to do: make it this sound less like an exact copy from<sup>8</sup>]

[to do: Results] We find that the anisotropy of the JP causes certain features to appear in and disappear from its scattering spectrum under certain orientations, particularly in the NIR range.

The scattering spectrum of the JP is qualitatively different from that of equivalently-sized Au spheres for all directions of illumination, though correspondences between some features exist.

Coarse-grained simulations for longer wavelengths (up to 1400 nm) suggest that the drop-off that was originally inferred in<sup>16</sup> does not manifest in actuality.

An experimental setup that can detect these features, possibly even track them in real time, is feasible.

Interesting things to do with this in the future might be...

- Direct analysis of the surface plasmons: Decomposition of the tangential electric field in an appropriate basis (vector hemispherical harmonics?) to find relative excitation of every (important) surface plasmon mode, depending on wavelength and illumination angle.

- Real-time spectroscopy to track a JP's out-of-plane angle.

[to do: Further investigation of the angular distributions could help develop a computationally inexpensive theory of the pressure cross-section of JPs.]

## Acknowledgements

[...] This measure is co-financed with tax revenue on the basis of the budget adopted by the Saxon State Parliament.

## Author Contributions

F.C. and F.H.P. designed the experiments; F.H.P. constructed the optical setup, performed the experiments, implemented the simulations and conducted the data analysis; F.H.P. wrote the manuscript; All authors reviewed the manuscript.

## Competing Interests

The authors have no competing interests to declare.

# Supporting Information Available

[...]

## References

- Graham, D.; Faulds, K. Plasmonic and photothermal properties of silica-capped gold nanoparticle aggregates. *The Journal of Physical Chemistry C* **2023**, *127*, 24475–24486.
- (10) Zhang, J.; Li, Z.; Bai, Y.; Yin, Y. Gold nanocups with multimodal plasmon resonance for quantum-dot random lasing. *Appl. Mat. Today* **2022**, *26*, 101358.
- (11) Zhang, Y.; Barhoumi, A.; Lassiter, J. B.; Halas, N. J. Orientation-preserving transfer and directional light scattering from individual light-bending nanoparticles. *Nano Lett.* **2011**, *11*, 1838–1844.
- (12) Chaudhari, K.; Pradeep, T. Spatiotemporal mapping of three dimensional rotational dynamics of single ultrasmall gold nanorods. *Sci. Rep.* **2014**, *4*, 5948.
- (13) Wagner, R.; Heerklotz, L.; Kortenbruck, N.; Cichos, F. Back focal plane imaging spectroscopy of photonic crystals. *Appl. Phys. Lett.* **2012**, *101*, 081904.
- (14) Wagner, R.; Cichos, F. Fast measurement of photonic stop bands by back focal plane imaging. *Phys. Rev. B* **2013**, *87*, 165438.
- (15) Mie, G. Beiträge zur Optik trüber Medien, speziell kolloidaler Metallösungen. *Annalen der Physik* **1908**, *330*, 377–445.
- (16) Patzschke, F. H. Orientation-dependent Spectroscopy of Plasmonic Janus Particles. 2023.
- (17) Gouesbet, G.; Gréhan, G. *Generalized Lorenz–Mie Theories*, second edition ed.; Springer: Heidelberg, 2017.
- (18) Johnson, P. B.; Christy, R. W. Optical Constants of the Noble Metals. *Phys. Rev. B* **1972**, *6*, 4370.
- (19) Bohren, C. F.; Huffman, D. R. *Absoprtion and Scattering of Light by Small Particles*, wiley professional paperback edition ed.; John Wiley & Sons: Weinheim, 1998; pp 82–129, 136.
- (1) Bregulla, A. P.; Cichos, F. Flow fields around pinned self-thermophoretic microswimmers under confinement. *J. Chem. Phys.* **2019**, *151*, 044706.
- (2) Auschra, S.; Bregulla, A.; Kroy, K.; Cichos, F. Thermotaxis of Janus Particles. *Eur. Phys. J. E* **2021**, *44*.
- (3) Selmke, M.; Khadka, U.; Bregulla, A. P.; Cichos, F.; Yang, H. Theory for controlling individual self-propelled microswimmers by photon nudging I: directed transport. *Phys. Chem. Chem. Phys.* **2018**, *20*, 10502.
- (4) Ilic, O.; Kaminer, I.; Zhen, B.; Miller, O. D.; Buljan, H.; Soljačić, M. Topologically enabled optical nanomotors. *Sci. Adv.* **2017**, *3*, e1602738.
- (5) Patzschke, F. H. Finite Elements Simulations of Optical Torques on Metal-Dielectric Janus Particles. 2020.
- (6) Mirin, N. A.; Halas, N. J. Light-Bending Nanoparticles. *Nano Lett.* **2009**, *9*, 1255–1259.
- (7) King, N. S.; Li, Y.; Ayala-Orozco, C.; Brannan, T.; Nordlander, P.; Halas, N. J. Angle-and spectral-dependent light scattering from plasmonic nanocups. *ACS Nano* **2011**, *5*, 7254–7262.
- (8) Islam, M. M.; Hosseini, M. M.; Koschny, T.; Hillier, A. C. Shape- and Orientation-Dependent Scattering of Isolated Gold Nanostructures Using Polarized Dark-Field Microscopy. *J. Phys. Chem. C* **2021**, *125*, 11478–11488.
- (9) Fergusson, J.; Wallace, G. Q.; Sloan-Dennison, S.; Carland, R.; Shand, N. C.;